EMMA-Tracker v1.0: A ~~lifecycle-based algorithm for identifying and tracking~~ mesoscale convective ~~systems in observations~~ system tracker and ~~climate models~~27-year European observational climatology

David Kneidinger[1], Armin Schaffer[2], and Douglas Maraun[3]

[1]Wegener Center for Climate and Global Change, University of Graz, Graz, Austria
[2]Wegener Center for Climate and Global Change, University of Graz, Graz, Austria
[3]Wegener Center for Climate and Global Change, University of Graz, Graz, Austria

Correspondence: David Kneidinger (david.kneidinger@uni-graz.at)

Abstract. ~~Understanding the long-term climatology and physical drivers of Mesoscale Convective Systems~~ Investigating how mesoscale convective systems (MCSs) ~~in Europe is hindered by the lack of multi-decadal datasets and the difficulties distinguishing precipitation resulting from MCSs from synoptic scale frontal precipitation. Reference datasets for model evaluation that mix these physically distinct phenomena can cause misinterpreting climate model skill in representation of mesoscale convective~~ over Europe will change in a warming climate relies on robust projections from climate models. To confidently use these projections, researchers must first understand model capabilities and uncertainties through strict, process-based evaluation against past observations. However, a lack of suitable reference datasets currently hinders this evaluation. Existing observational trackers often use variables unavailable in European climate model ensemble output or group mesoscale convection together with co-occurring synoptic-scale fronts. Because climate models represent synoptic and mesoscale dynamics through fundamentally different physical pathways, accurately evaluating a model's convective performance requires a benchmark that strictly isolates mesoscale processes. To address this, we introduce the EMMA-Tracker (Evolution-based MCS Model Assessment), ~~a novel algorithm designed to identify and track MCSs~~ an algorithm purpose-built to evaluate models using only standard ~~model~~ output variables. ~~This intentional design choice enables a physically consistent comparison between observations and climate model ensembles, providing a pathway to investigate how MCS characteristics may evolve in a warming climate through the analysis of future projections.~~ We apply this tracker to IMERG precipitation and ERA5-derived atmospheric instability to generate a 27-year (1998–2024) warm-season ~~climatology—~~ climatology —the longest reference dataset of European MCSs to date. ~~The algorithm's core innovation is a series of physics-based~~

Following the initial tracking, EMMA applies post-processing filters ~~that utilize the system's full spatiotemporal lifecycle to isolate coherently propagating MCSs from stationary thunderstorms and frontal rainbands~~to retain only distinct MCSs, systems that maintain a clear shape and steady movement, remaining structurally distinct from any co-occurring synoptic triggers. Our results show that these ~~coherent~~ distinct MCSs are the dominant driver of extreme hourly precipitation. Their contribution to hourly warm season precipitation systematically increases with hourly precipitation intensity, ~~exceeding~~ accounting for over 60% of heavy precipitation (P99.9) across most of continental Europe and 80% over parts of the Mediterranean. The EMMA-

Tracker provides both an observational reference for climatological studies and ~~for a~~ targeted, process-oriented ~~evaluation of~~ benchmark for evaluating regional and convection-permitting climate models.

1 Introduction

Mesoscale ~~Convective Systems~~ convective systems (MCSs) are a principal driver of high-impact weather across Europe, frequently leading to heavy precipitation, damaging winds, and large hail that pose substantial societal and economic risks (Da Silva and Haerter, 2023; Schumacher and Rasmussen, 2020; Surowiecki and Taszarek, 2020). For instance, on 18 August 2022, a violent, long-lived convective system known as a derecho swept from the Balearic Islands across Corsica, Italy, and Austria, producing measured wind gusts up to 62.2 $\mathrm{m\,s^{-1}}$ (224 $\mathrm{km h^{-1}}$) and extreme precipitation values, causing 12 fatalities, and leaving a trail of destruction over 1000 km long (Fery and Faranda, 2024; Pucik et al., 2022; Gatzen and Pucik, 2023).

~~The accurate simulation of MCSs is therefore a critical benchmark for the skill of climate models, used for modelling the influence of climate change on these heavy precipitation and strong wind events. Yet it remains a grand challenge that exposes~~ Given the devastating impacts of such extreme events, understanding how the characteristics of MCSs will evolve in a warming climate is critical. Climate models are our primary tools for projecting these changes, yet accurately simulating the complex spatiotemporal organization of MCSs remains a well-documented grand challenge (Feng et al., 2021b; Lin et al., 2022). Consequently, there is a crucial need for more sophisticated, process-based model evaluation.

The scientific community is moving beyond simple bias maps toward assessing whether models can reproduce the physical processes that lead to high-impact weather, as this process-understanding is fundamental to building trust and generating robust climate information (Doblas-Reyes et al., 2021; Eyring et al., 2019). Regional Climate Models (RCMs), such as those in the Coordinated Regional Downscaling experiment (EURO-CORDEX) ensemble (Jacob et al., 2014, 2020) (0.11°, $\sim$ 12.5 km resolution), rely on convective parameterizations and exhibit persistent biases, including an underestimation of hourly precipitation extremes and a premature triggering of the diurnal precipitation cycle (Prein et al., 2015; Meredith et al., 2021; Kotlarski et al., 2014; Hohenegger et al., 2009). The recent advent of convection-permitting model (CPMs) in ensembles like EURO-CORDEX FPS on Convective phenomena at high resolution over Europe and the Mediterranean (FPS-CONV; Coppola et al. (2020)) ($\sim$3 km resolution) marks an important advancement by explicitly resolving deep convection, leading to marked improvements in hourly precipitation characteristics (Ban et al., 2021; Kendon et al., 2017). Even CPMs can still produce overly intense and spatially confined convective cells and exhibit biases in storm location, underscoring the continued need for robust, process-oriented observational benchmarks for evaluation (Fosser et al., 2015; Kendon et al., 2021).

Recent high-resolution modeling studies investigating MCSs in a future climate have yielded mixed signals regarding their frequency, preventing simple generalizations across regions. While some convection-permitting simulations project widespread increases in MCS frequency over North America (Prein et al., 2017; Cui et al., 2024), others identify a stagnation or non-significant decrease in specific hotspots, such as the US Great Plains (Haberlie and Ashley, 2019) and the Amazon basin (Rehbein and Ambrizzi, 2023). Despite this regional heterogeneity in occurrence, there is a consensus that they might get more intense in a warming climate (Schumacher and Rasmussen, 2020; Prein et al., 2017; Dougherty et al., 2023). However, the

transferability of these findings is limited by the strong sensitivity of MCS simulations to region-specific model configurations (Prein et al., 2022), underscoring the necessity for a dedicated European evaluation. A prerequisite for such an analysis is the creation of a robust observational benchmark.

~~The development of such a~~ Developing a robust benchmark for Europe is ~~complicated by a fundamental meteorological characteristic: the prevalence of~~ difficult because synoptic-scale atmospheric fronts associated with mid-latitude cyclones ~~. This front-dominated climate creates a methodological conundrum~~frequently occur in the region (Catto et al., 2014; Hénin et al., 2019; Schaffer . Past literature attributes European precipitation extremes to different phenomena depending on the timescale. While some studies suggest ~~MCSs are the primary drivers of~~ mesoscale convective systems (MCSs) primarily drive hourly precipitation extremes during the warm season (Da Silva and Haerter, 2023), other ~~work focusing specifically on~~ research shows cold fronts also ~~identifies them as responsible for~~ trigger a large fraction of ~~hourly extreme precipitation over Europe~~ these hourly events (Schaffer et al., 2024). Furthermore, ~~studies analyzing precipitation extremes over~~ when analyzing longer timescales (e.g., 6-hourly)~~find that a large majority of such events in the mid-latitudes are directly associated with atmospheric fronts (Catto and Pfahl, 2013). This highlights that different systems can dominate precipitation extremes depending on the timescale and season. Existing detection methods may not be adequately distinguishing between two physically distinct phenomena. An MCS is defined by its self-sustaining mesoscale dynamics (meso-β scale, 20–200), where internal processes like cold pools govern its evolution and propagation (Schumacher and Rasmussen, 2020). In contrast, frontal precipitation is dynamically forced by convergence along a synoptic-scale boundary (meso-α, 200–1000 to synoptic scale) (Markowski and Richardson, 2011) . Climate models represent these processes through fundamentally different pathways—parameterized sub-grid scale convection versus explicitly resolved grid-scale dynamics in RCMs. An evaluation dataset that conflates these two systems risks a profound misdiagnosis of model performance, particularly as models that better resolve processes like frontal dynamics may show apparent improvements unrelated to changes in convective representation (Kendon et al., 2017).~~ , atmospheric fronts directly cause the vast majority of mid-latitude precipitation extremes (Catto and Pfahl, 2013). As recent global quantifications demonstrate, these different attributions are not contradictory, because extreme precipitation can result from events where fronts and MCSs co-occur (Tsai et al., 2025), and large-scale frontal ascent frequently forces organized convection (Schumacher and Rasmussen, 2020) .

~~For instance, an analysis using such~~ Although fronts and MCSs coexist in nature, evaluating climate models requires researchers to cleanly separate their physical structures. If an observational reference dataset mixes these two systems, the evaluation process can become fundamentally flawed. Because Europe's precipitation climatology is heavily front-dominated, the environmental signal in any mixed dataset can become overwhelmingly dictated by large-scale baroclinic forcing. Even coarse-resolution RCMs represent these broad baroclinic dynamics reasonably well (Prein et al., 2015; Schaffer et al., 2025). However, accurately simulating the severe, short-duration hazards characteristic, such as the severe wind gusts of convective lines usually require convection-permitting scales (Kendon et al., 2017). Consequently, if researchers generate storm-centered composites or analyze environmental conditions using a mixed dataset~~might erroneously conclude that moving from a parameterized RCM to a CPM provides little improvement in simulating MCSs, simply because the dataset was dominated by well-resolved frontal systems, missing the true (and potentially large) improvement in the simulation of mesoscale convective physics. For~~

~~the specific purpose of diagnosing and improving model physics, it is therefore imperative to distinguish systems dominated by internally-driven mesoscale organization from those governed by externally-forced synoptic precipitation .~~

~~This challenge exposes the limitations of existing MCS identification methodologies for the specific task of process-based model evaluation in Europe. While several objective tracking algorithms have recently been developed to identify MCSs in both observations and simulations, such as the Tracking Algorithm for Mesoscale Convective Systems (TAMS; Núñez Ocasio and Moon (2024)) and the Python FLEXible object TRacKeR (PyFLEXTRKR ; Feng et al. (2023)) , most methods rely on satellite-derived brightness temperature thresholds (Feng et al., 2025). The pioneering climatology of Morel and Senesi (2002), identifies systems by their large, cold cloud shields. However, infrared brightness temperature is not a~~ the well-resolved synoptic features dominate the signal, making RCMs and CPMs appear structurally similar. This baroclinic dominance completely masks the intense, localized physics of organized convective storms, which often develop in entirely different environments such as the prefrontal warm sector citepnhess-23-3703-2023. However, separating these systems is inherently difficult when their cloud and precipitation footprints become contiguous. Historically, tracking methods identified systems by their large, cold cloud shields, as demonstrated in the European climatology of Morel and Senesi (2002). While early methods sometimes confused active convection with non-precipitating cirrus anvils (Fiolleau and Roca, 2013), recent algorithms (e.g., TAMS (Núñez Ocasio and Moon, 2024) and PyFLEXTRKR (Feng et al., 2023)) have significantly improved detection by incorporating precipitation data alongside infrared brightness temperature (Feng et al., 2025, 2021a). Yet, relying on infrared brightness temperature or outgoing longwave radiation (OLR) creates a fundamental barrier for evaluating climate models. Because regional climate model ensembles have historically lacked hourly OLR output, researchers cannot use these advanced trackers for a consistent, pan-European assessment of simulated MCSs. To diagnose climate model physics accurately, we need a tracking framework that structurally isolates organized mesoscale convection using only standard model output ~~variable, and cold cloud tops often conflate active convection with non-precipitating cirrus anvils (Fiolleau and Roca, 2013).~~ variables.

Regional climatologies have successfully characterized MCS archetypes over specific areas, such as Poland (Surowiecki and Taszarek, 2020), the Mediterranean (Rigo et al., 2019; Kolios and Feidas, 2010), and Spain (García-Herrera et al., 2005). More recently Da Silva and Haerter (2023) studied convective Systems over Europe using satellite-based precipitation and lightning data for identification. Their work, which purposefully includes convectively active frontal systems to characterize all large organized precipitation, restricts the ability to diagnose process-level model biases. Moreover, these studies generally rely on variables that are not standard output in most climate model ensembles, preventing a consistent pan-European assessment.

To address these ~~critical gaps, this paper introduces~~ gaps, we introduce the EMMA-Tracker ~~algorithm and the resulting~~ (Evolution-based MCS Model Assessment) and a 27-year (~~1998–2024) climatology. The purpose is to provide a robust, physically-consistent reference dataset of genuine MCSs , specifically tailored for the evaluation of RCMs and CPMs over Europe~~1998–2024) European reference climatology. This dataset provides a physically consistent benchmark of MCSs for evaluating regional and convection-permitting models. The EMMA-Tracker is a python-based algorithm designed to identify and track MCSs using hourly precipitation and atmospheric instability fields. The core novelty of the ~~EMMA-Tracker lies in a series of~~ tracker lies in physics-based ~~post-processing filters that enforce a strict conceptual model of~~ filters that identify an MCS as ~~an organized, self-sustaining convective system that propagates coherently and independently of its initial trigger.~~

systems that maintain a clear shape and steady movement, remaining structurally distinct from any co-occurring synoptic triggers.

This paper is structured as follows: Section 2 details the input datasets and the multi-stage EMMA-Tracker algorithm. Section 3 presents a validation of these filters, demonstrating their effectiveness in separating MCSs from frontal systems and stationary thunderstorms. The resulting 27-year MCS climatology is presented in Section 4, focusing on spatial distribution, system characteristics, and contribution to heavy hourly precipitation. Section 5 concludes the implications and limitations of the methodology and dataset.

2 Data and Methods

2.1 Observational Datasets

2.1.1 Integrated Multi-satellitE Retrievals for GPM (IMERG)

The precipitation data for this study were sourced from the IMERG Version 7 "Final Run" product (Huffman et al., 2019). IMERG provides quasi-global precipitation estimates by synthesizing data from the GPM satellite constellation, primarily merging passive microwave sensor data with microwave-calibrated infrared observations. The "Final Run" is a research-grade dataset that undergoes a month-to-month bias adjustment using monthly gauge analyses from the Global Precipitation Climatology Centre, making it the most accurate IMERG product available (O et al., 2017).

We used the data on its native grid of $0.1^\circ \times 0.1^\circ$ in a European domain (30° to 70° N, -20° to 40° E). Although available at a 30-minute resolution, we used an hourly resolution to ensure direct comparability with the temporal resolution of most climate model precipitation outputs.

The primary reason for selecting IMERG is its fine spatial resolution, which is superior to many reanalysis products and crucial to resolving small-scale precipitation structures and heavy sub-daily precipitation, that are a vital input for our storm detection algorithm. IMERG-Final exhibits improved detection of extreme rainfall events, especially during summer, and performs more reliably at daily resolution when compared to ECMWF Atmospheric Reanalysis Version 5 (ERA5) (Mohammed et al., 2025). Despite its established robustness (Pradhan et al., 2022), we acknowledge known regional limitations. For example, validation studies in Europe show IMERG can underestimate precipitation in mountainous regions like the Alps and Scandinavian mountains, while overestimating it over areas such as the British Isles and the Italian Peninsula (Navarro et al., 2019).

However, since our analysis focuses on the spatio-temporal structure and MCS precipitation contribution rather than absolute precipitation volumes, these biases are considered acceptable. ~~The~~ We chose IMERG based on its ability to accurately capture the morphology of precipitation plumes ~~was the main factor in our choice~~ when evaluated against the Integrated Nowcasting through Comprehensive Analysis (INCA) (Figure S3). Furthermore, IMERG is a well-established dataset for tracking various storm types, including MCS, providing a strong precedent for its application in this work (Feng et al., 2021a; Da Silva and Haerter, 2023; Hayden et al., 2021).

Finally, we acknowledge a known limitation of the IMERG product at high latitudes, due to the oblique viewing angle of geostationary satellites, this high-frequency infrared input is generally unavailable or degraded poleward of approximately 60° N (Huffman et al., 2019). Consequently, while our tracking domain extends to 70° N to capture most of the Scandinavian landmass, the tracked systems in these high-latitude regions are subject to higher uncertainty and results there should be interpreted with this limitation in mind.

2.1.2 ECMWF Atmospheric Reanalysis Version 5 (ERA5)

Atmospheric fields required for the calculation of convective instability were sourced from ERA5 (Hersbach et al., 2023).

For this study, hourly temperature and specific humidity data were extracted on four pressure levels—925, 850, 700, and 500 hPa —to compute the lifted index (LI) across the European domain (30° to 70° N, -20° to 40° E) for the full 1998–2024 time span. For height contours in the map plots, ~~IMERG~~ ERA5 geopotential is used.

2.2 EMMA-Tracker

The EMMA-Tracker is designed to identify and track convective storm systems from gridded datasets. The methodology is executed in four main stages: (1) preprocessing of input data to derive an atmospheric instability index, (2) a multi-step detection algorithm to identify MCS candidates based on their precipitation structure and convective nature, (3) the tracking of the detected MCS candidates and (4) the postprocessing filter to filter system with non MCS characteristic propagating life cycle behavior.

2.2.1 Algorithm Input and Preprocessing

The algorithm requires two primary inputs at an hourly frequency: precipitation fields from IMERG and atmospheric data from IMERG. The IMERG data is used exclusively to diagnose the potential of the atmospheric environment for convection.

To quantify convective instability, we calculate the LI. This index was chosen over convective available potential energy (CAPE) for two main reasons: First, CAPE is not a standard output variable in many regional climate model ensembles, such as EURO-CORDEX (EURO-CORDEX, 2022). Second, the LI is a relative measure between pressure levels, making it less sensitive to systematic temperature or humidity biases that may be present in a given model or reanalysis dataset.

The LI is calculated from hourly IMERG temperature and specific humidity data on the 925, 850, 700, and 500 hPa pressure levels. We follow the methodology of Púčik et al. (2017), which defines the LI as the difference between the environmental temperature at 500 hPa and the temperature of a parcel lifted moist-adiabatically to that level. This method includes a virtual temperature correction to account for effect of moisture on air density and identifies the most unstable parcel by testing source layers at 925, 850, and 700 hPa. The lowest resulting LI value is selected, ensuring that the source layer is always above the model topography. Negative LI values indicate latent instability and an increased potential for deep convection. The LI is then regridded to the 0.1° grid of the IMERG dataset to ensure spatial coherence between the datasets. This was performed using bilinear interpolation.

2.2.2 MCS Detection Algorithm

We detect MCS candidates independently at each hourly timestep. This approach allows for parallel processing of the data, which significantly enhances computational efficiency and makes the algorithm suitable for analyzing large, multi-decadal climate datasets and ensemble data. Prior to the first step, a mild spatial smoothing is applied to the IMERG precipitation field using a Gaussian filter with a standard deviation of one grid box ~~to reduce small-scale grid noise~~ (Fig. 1a). This acts as a spatial low-pass filter to address grid-scale patchiness, ensuring the threshold-based connected-components algorithm identifies large convective cores as unified structures rather than artificially fracturing them. The detection process then consists of three main steps, which are illustrated for an example event (Fig. 1 b-d).

1. Identification of Convective Cores: First, the smoothed IMERG precipitation field is masked using a heavy precipitation threshold to isolate the most intense rainfall regions, which are considered the convective cores of potential storm systems. To ensure the EMMA-Tracker is transferable for process-based climate model evaluation, this threshold is defined not as a fixed value but as a high percentile of the dataset's own precipitation distribution. This relative approach automatically adapts to the specific climatology and systematic biases of any given observational or model dataset.

   For this study, we define the heavy precipitation threshold as the domain wide 99th percentile of all wet hours > 0.1 $\mathrm{mm\,h^{-1}}$ during the warm season (May-September) over the full European domain (30° to 70° N, -20° to 40° E). This methodology is consistent with studies that use similar percentiles to classify hourly heavy precipitation in Europe, which are almost entirely generated by convective processes (Haslinger et al., 2025; Berg et al., 2013). In the observational IMERG dataset, this 99th percentile corresponds to an absolute threshold of 6.8 $\mathrm{mm\,h^{-1}}$. The resulting binary mask of convective cores is then processed using a connected-components labeling algorithm with 8-connectivity to group adjacent pixels into distinct heavy precipitation plumes (Fig. 1b), which are required to be at least four pixels, to exclude isolated noisy pixels.

2. System ~~Merging~~Segmentation: To connect distinct but related convective cores into a single, coherent storm system, the algorithm identifies contiguous envelopes of moderate precipitation > 1 $\mathrm{mm\,h^{-1}}$. Unlike the convective core threshold, a fixed value is retained here because of IMERGs known wet bias at low intensities, where the product tends to produce a significant number of "false alarm" pixels with very light precipitation (Cui et al., 2020). Any distinct convective cores that fall within the same contiguous moderate precipitation envelope are grouped together into a single entity. This step allows the algorithm to group multi-core systems or connect convective lines with their associated stratiform rain regions (Fig. 1c).

3. Convective Systems: Finally, each identified storm candidate is characterized by its convective nature. The LI field is spatially overlaid with the storm's precipitation footprint. If at least 10% of the storm's total area has an LI value below -2 K, the entire system is flagged as "convective" (Fig. 1d). Because precipitation is an accumulated variable in model data and LI is an instantaneous snapshot, the algorithm evaluates the LI at the beginning of the precipitation

accumulation period. This ensures the pre-storm environment is assessed before the convective event consumes the atmospheric instability.

The resulting systems are considered storm candidates. These candidates are first filtered by a minimum area threshold to reduce computational load in the subsequent tracking stage by eliminating very small features. This minimum area threshold was chosen as 10 grid boxes. An optional secondary filter can be applied to select systems based on the number of distinct convective cores they contain, which can help differentiate between single-cell storms and more complex, multi-cellular linear systems. For this study, this filter is set to a minimum of one core.

All identified storm candidates, along with their properties (i.e., size, location, convective flag), are stored for each timestep, providing the input for the tracking stage of the algorithm.

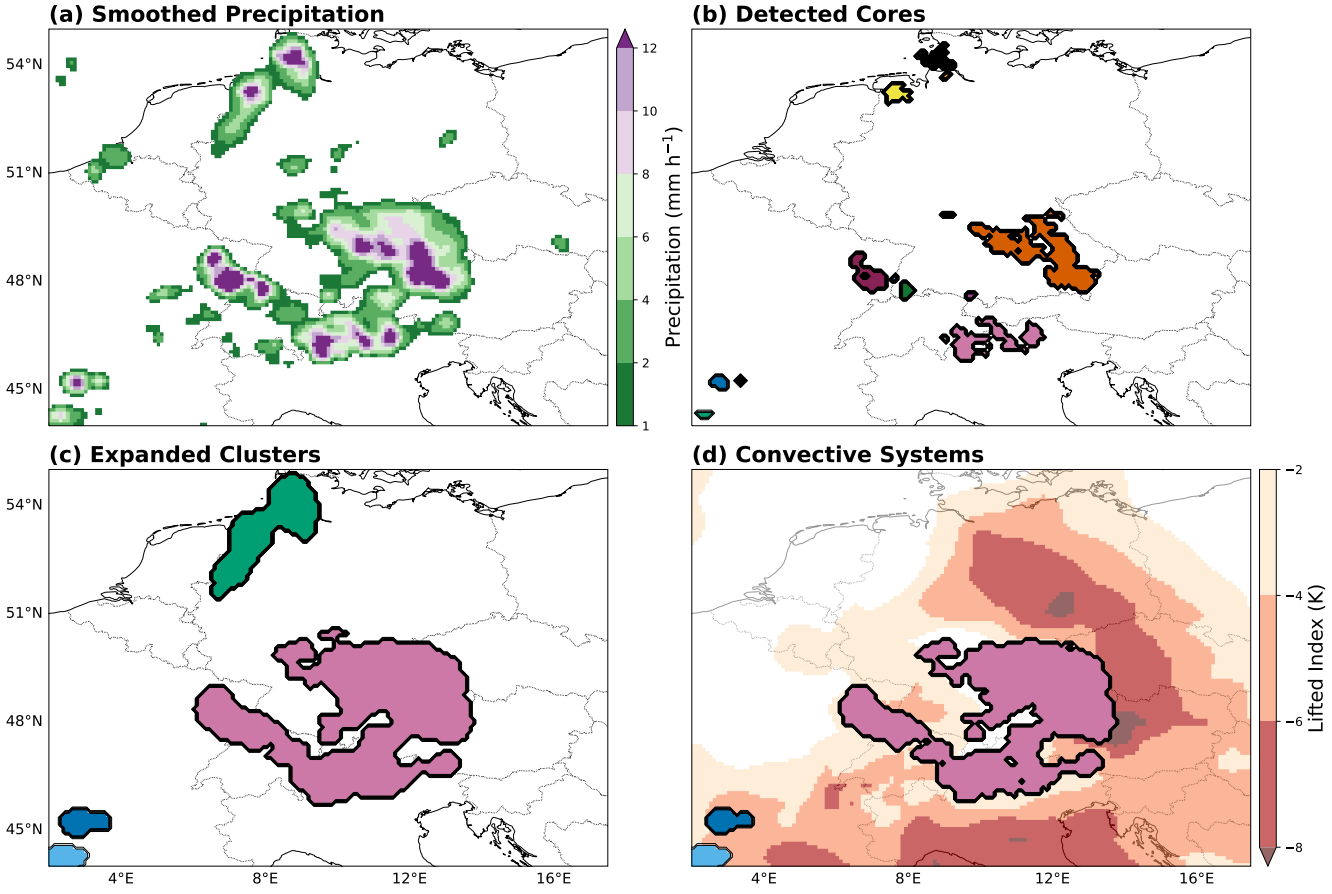

Figure 1. Illustration of the EMMA detection algorithm steps for a MCS over central Europe on 11 July 2023 at 23:00 UTC. (a) IMERG precipitation field after applying a Gaussian filter for smoothing. (b) Identified convective cores using a heavy precipitation threshold, with individual clusters shown in different colors. (c) Expanded and merged clusters using a moderate precipitation threshold. (d) Resulting convective storm candidates,satisfying the LI criterion, overlaid on the LI field.

2.2.3 Tracking and MCS Identification

The second stage of the EMMA-Tracker links the storm candidates identified at individual timesteps into temporally coherent tracks. The core of the tracking methodology relies on the spatial overlap of storm candidates between consecutive hourly frames, a well-established technique for tracking precipitating systems, provided the temporal resolution is sufficient to resolve their movement (Feng et al., 2023). This reliance on hourly data was a key consideration, ensuring the algorithm's applicability to standard climate model output.

The tracking process assigns a unique track ID to each new storm candidate and attempts to propagate that ID forward in time based on the following ordered logic. In all three cases, a link is only established if the precipitation areas overlap by at least 10%:

1. Continuity: A tracked system at time t is linked to a candidate at time $t+1$ if their precipitation areas overlap with at least 10 %. The candidate at $t+1$ inherits the track ID of the system from time t. (Fig. 2a)

2. Merging Events: If multiple tracked systems at time t overlap with a single, candidate at $t+1$, it is classified as a merging event. The track ID of the largest system from time t is propagated to the merged candidate at $t+1$. The tracks of the smaller systems are terminated at time t, but their association with the primary track is recorded. (Fig. 2b)

3. Splitting Events: If a single tracked system at time t overlaps with multiple candidates at $t+1$, it is considered a splitting event. The track ID is continued with the candidate at $t+1$ that has the largest area, while the smaller candidates are initialized as new, independent tracks. (Fig. 2c)

For tracked systems at time t that do not have an overlapping candidate at $t+1$, a second check is made. Following Moseley et al. (2013), the algorithm calculates a mean displacement vector from nearby systems, within a 1000 km radius, to extrapolate the position of the lost system. If this extrapolated position overlaps with an unassigned candidate at $t+1$, the track is rescued and continued. This step is performed to reduce the identification error of very fast moving systems. The total effect of this rescue step is found to be minimal, but was included for completeness.

After the tracking is complete for all timesteps, a final classification is performed to identify which tracks qualify as MCS. A tracked system is classified as an MCS if it meets a minimum size criterion of 3500 km^2 for a continuous duration of at least four hours, a common threshold for MCS persistence (Feng et al., 2021a). Furthermore, a sensitivity analysis (Figure ~~S1~~S2) confirms that the resulting climatology is robust to this specific threshold, with only minor variations in the number of identified tracks across values ranging from 2000 to 7000 km^2. We define the contiguous period during which a track meets these criteria as its mature phase. Furthermore, a valid MCS must be flagged as "convective" for at least one timestep during its mature phase. An schematic example of these tracking steps, based on an MCS from 11 July 2023 is shown in Figure 2d.

The final output of the algorithm stores two primary data products: (1) the full lifecycle track for every identified MCS, from its initial detection to its final dissipation, and (2) the isolated mature phase of each MCS. Information on all merging and splitting events associated with a mature MCS is also retained, allowing for detailed analysis of the system's evolution.

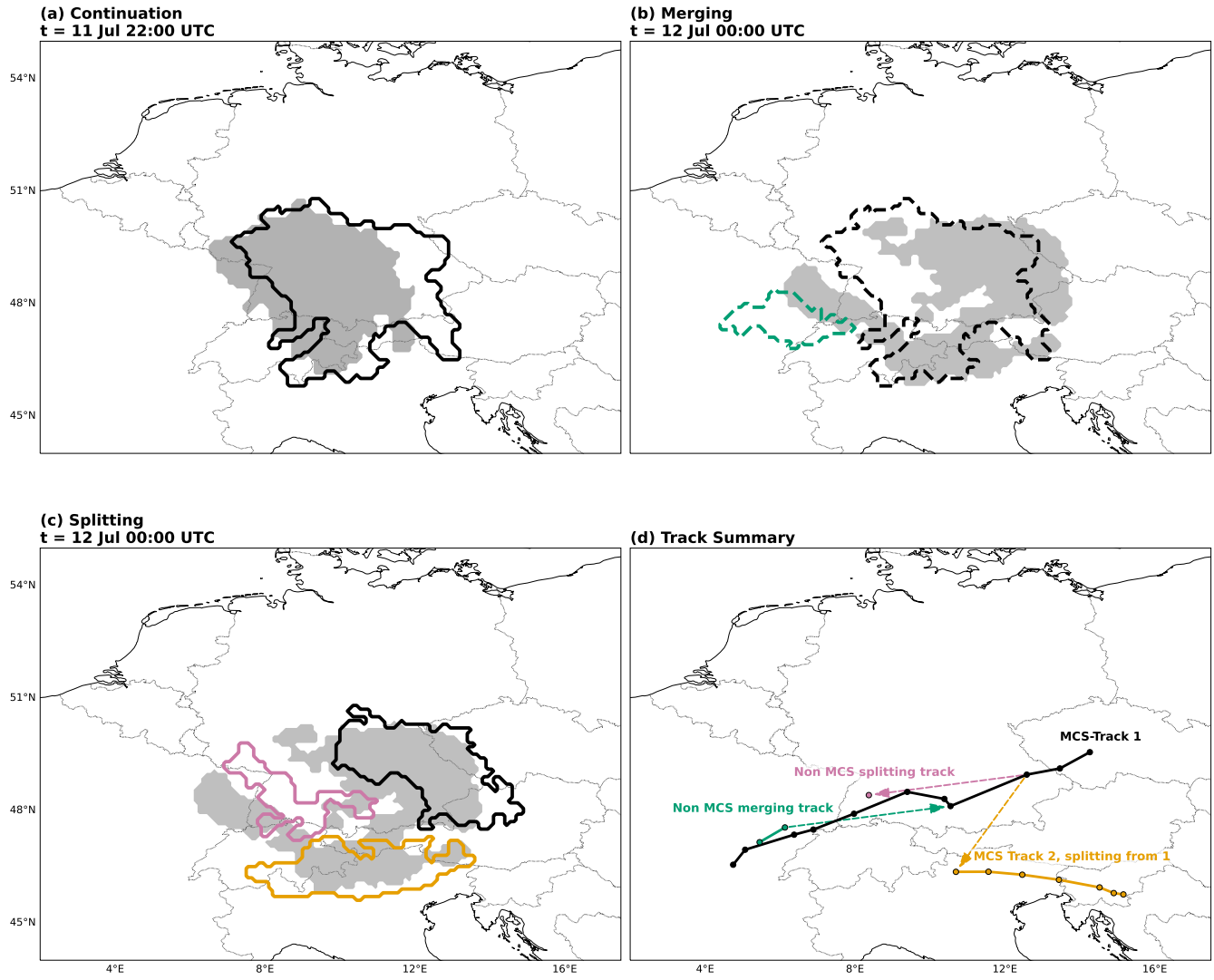

Figure 2. Schematic illustration of the EMMA tracking algorithm logic, 11 July 2023 (continuation, merging, splitting). Note: This example is derived from a sensitivity run with reduced smoothing to visually ~~highlight~~ show the ~~topological splitting and~~ merging ~~operations~~in panel (b) based on this real world Derecho event. In panels (a-c), the state of a system at a reference time t is shown by a filled precipitation mask, the state at $t-1$ by dashed contours, and the state at $t+1$ by solid contours. The reference time t for each panel is given in the title.

(a) Simple continuation, showing the system's position at $t-1$ (dashed) and its updated position with precipitation at t. (b) A merging event, where two parent systems at $t-1$ (green and black dashed contours) combine into a single system at t (precipitation mask). (c) A splitting event, where the parent system at t (precipitation mask) divides into multiple child systems at $t+1$ (black, magenta and orange solid contours). (d) A summary of the full precipitation-weighted track histories for the systems involved, showing the paths of the main MCS track and the associated non-MCS merging and splitting tracks.

2.2.4 Postprocessing Filters for MCS Candidate Refinement

Following the tracking stage, we apply a series of postprocessing filters to the identified MCS candidate systems. A core novelty of the EMMA-Tracker is ~~that these filters operate on the full spatiotemporal lifecycle of the system, rather than relying solely on instantaneous properties available during the initial detection phase~~how it evaluates the system's entire lifecycle. Rather than just checking if a storm meets static size thresholds for a few hours, EMMA assesses the storm's physical behavior, such as its track straightness and step-by-step area changes, at every single timestep. Together, these filters ensure that the final dataset represents a physically consistent and robust climatology of MCSs, crucially distinguishing them from synoptic-scale frontal precipitation. This separation is vital for the evaluation of how climate models represent organized mesoscale convection. It is important to note that the specific thresholds for these filters have been empirically tuned for the European domain based on a sensitivity analysis (Figure ~~S2~~S3) and event cases which assessed the impact of each filter on the total number of accepted MCS tracks. While the filtering concepts are generalizable, their direct application to other regions may require careful recalibration. The postprocessing routine consists of three distinct filters applied to each track.

- Track Straightness: ~~Genuine MCSs~~ The distinct MCSs the EMMA-Tracker aims to identify are characterized by coherent propagation, which distinguishing them from stationary or erratic precipitation features. To enforce this, we calculate a track straightness index. This filter effectively removes two primary types of false positives: quasi-stationary convection anchored to orography (Fig. A1a) and synoptic fronts whose centroids shift erratically as different parts of the frontal system are detected (Fig. A1b). This dimensionless metric is defined as the ratio of the net displacement to the total path length:

  $$\text{straightness} = \frac{\|\boldsymbol{x}_{\text{end}} - \boldsymbol{x}_{\text{start}}\|}{\sum_{t=\text{start}}^{\text{end}-1} \|\boldsymbol{x}_{t+1} - \boldsymbol{x}_t\|}$$

  where $\boldsymbol{x}_t$ is the coordinate vector of the system's precipitation-weighted centroid at time t. A value approaching 1 indicates a highly linear trajectory, while a value near 0 signifies erratic or completely stationary behavior. Systems that have an overall short displacement, but maintain a coherent propagation pattern, such as quasi stationary MCS or backbuilding MCSs, can still make it through the filter. A threshold of 0.4 was selected based on the distribution of straightness values across all initial tracks (Figure S2a). This value sits near the elbow point of the sensitivity curve, effectively separating the population of erratically moving or stationary systems from those with more coherent propagation.

- Environmental Instability Constraint: While the tracking algorithm requires a system to be flagged as "convective" for at least one timestep, true MCSs typically propagate within and are sustained by a persistently unstable airmass. We therefore enforce that a track is only retained if the mean LI, averaged over its full duration, remains at or below 1.5 K. This choice is strongly supported by the sensitivity analysis (Figure S2b), where the number of accepted MCS tracks nearly saturates for mean LI values ≥ 1.5 K. This plateau indicates that 1.5 K effectively separates the vast majority of identified systems, existing in neutral or unstable mean environments, from a small population persisting in more stable mean conditions, which are unlikely to represent ~~genuine self-sustaining~~ distinct MCSs. This filter is particularly

effective at removing long-lived frontal systems that may traverse a pocket of instability but are, on average, located in less convective favorable environments (Fig. A1c).

~~Genuine MCSs typically exhibit a smooth evolution in spatial extent during their lifecycle. To distinguish this natural~~

– Area Volatility: While distinct MCSs typically follow a smooth upscale growth and decay ~~from the~~ lifecycle, the precipitation fields of large-scale frontal systems often appear fragmented to a tracking algorithm. This fragmentation leads to rapid, physically implausible ~~size fluctuations often associated with frontal detection artifacts or spurious mergers~~fluctuations in the detected area as separate clusters are merged or split. To distinguish these diagnostic tracking artifacts from the natural evolution of organized convective systems, we apply an area volatility filter. This metric quantifies the squared change in area relative to the mean area between consecutive timesteps.

$$\text{volatility} = \frac{(A_{t+1} - A_t)^2}{0.5\,(A_{t+1} + A_t)}$$

with A_t the area of a system at time t. We remove systems exceeding a threshold of 9.0×10^4 km^2 at any point during the lifetime. As shown in the sensitivity analysis (Figure S2c), the number of accepted tracks becomes nearly insensitive to the threshold for values above this point. This flattening of the curve indicates that the filter is primarily removing a small population of tracks with extreme, physically implausible size fluctuations characteristic of frontal systems (Fig. A1d) or spurious merging of local thunderstorms.

3 Effectiveness of the Postprocessing Filters

This section demonstrates the spatial effect of each filter and provides a quantitative validation of their role in separating organized mesoscale convection from other precipitation phenomena.

Fig. 3 spatially illustrates the impact of this filtering cascade. The unfiltered warm-season climatology (Fig. 3a), which includes all tracked systems meeting the initial size, duration and convection criteria, shows high event frequencies in known convective hotspots, such as the Alps and the Balkan region (Galanaki et al., 2018; Taszarek et al., 2019). ~~However, it also features a prominent maximum over the~~ Fewer systems are tracked over North Atlantic, Great Britain, and the North Sea. This latter region coincides with the main North Atlantic storm track, which is dominated by synoptic-scale frontal precipitation (Dong et al., 2013; Rüdisühli et al., 2020; Catto and Pfahl, 2013). ~~The inclusion of these systems is a direct and expected consequence of our inclusive detection methodology, which relies on a low precipitation threshold (1 mm h^{-1}). The~~ Fig. 3e, which shows the relative effect of all combined filters, shows that the subsequent filters physically distinguish and remove these synoptic-scale systems.

The track straightness filter has the most significant quantitative impact, removing a large number of systems from both the Alpine region and the North Atlantic storm track (Fig. 3b). This filter effectively targets two distinct types of non-MCS phenomena. First, over complex orography, the inclusive precipitation threshold can artificially merge nearby, quasi-stationary

orographic precipitation cells. These merged objects may meet the area and duration criteria but fail to propagate coherently, resulting in a low straightness index. Second, over the storm track, the precipitation-weighted centroid of large, frontal rainbands can jump erratically as different embedded precipitation cells intensify and wane, also leading to a low straightness index and subsequent removal. We acknowledge that this filter may also remove some ~~genuine~~ MCSs embedded in frontal systems (e.g., squall lines). This is a deliberate methodological choice to ensure the final dataset is not contaminated by synoptic-scale systems, which is essential for our objective of evaluating model physics at the mesoscale.

The mean LI filter, which removes systems existing in, on average, stable environments (mean LI > 1.5 K), has its strongest relative impact over the North Atlantic, further removing systems over the storm track region (Fig. 3c). Finally, the area volatility filter (Fig. 3d) acts as a clean-up step, removing remaining spurious tracks, particularly over the Norwegian coast and the North Sea. These systems exhibit physically implausible, rapid fluctuations in size, characteristic of the detection algorithm intermittently merging and splitting large, parts of frontal rainbands as well as orographic triggered local convection (Fig. S4). The combined effect of all three filters (Fig. 3e) results in a final, refined MCS climatology (Fig. 3f) that is concentrated over continental Europe and key orographic regions, in strong agreement with the infrared-based climatology by Morel and Senesi (2002).

To quantitatively validate the effectiveness of the postprocessing filters in separating propagating MCSs from frontally-associated systems, we collocated all identified system timesteps (accepted and rejected) with an independent hourly frontal database of both cold and warm fronts, based on IMERG (Schaffer et al., 2024). A system's timestep is marked as frontal if its precipitation mask (> 1 mm h^{-1}) overlaps with any frontal pixel from the database. Fig. 4 presents the results of this collocation analysis over the 1998–2020 period covered by the frontal database.

The spatial distribution of the accepted MCS timesteps (Fig. 4a) shows the highest counts concentrated over continental Europe, particularly along the Alps, the Dinaric Alps, and parts of France and Germany, consistent with the final climatology (Fig. 3f). The corresponding frontal ratio for these accepted systems (Fig. 4b), calculated as the fraction of timesteps coinciding with a front, is generally low across these central European hotspots. Higher frontal ratios for accepted systems are observed over maritime regions like the North Sea and parts of the Mediterranean, as well as areas adjacent to the primary storm track.

The spatial distribution of the total count of rejected timesteps (Fig. 4c) exhibits prominent frontal contribution over the North Atlantic, the North Sea, and extending across the British Isles, directly coinciding with the typical North Atlantic storm track region. Primary maxima of rejected systems are found over the Alps, the Balkans, and parts of the Mediterranean. Examining the frontal ratio specifically for these rejected systems (Fig. 4d) reveals overwhelmingly high values over the North Atlantic and North Sea, frequently exceeding 80% in most areas. High frontal ratios among rejected systems are also evident over the rest of continental Europe.

These contrasting patterns between accepted and rejected systems provide strong validation for the filtering methodology. The filters successfully retain systems primarily over continental Europe where the precipitation associated with fronts is lower in the warm-season (Rüdisühli et al., 2020) (Fig. 4a, b). A large number of systems (Fig. 4c), particularly over the North Atlantic storm track, that are confirmed to be overwhelmingly associated with fronts (Fig. 4d) are effectively removed. This demonstrates the filters ability to isolate the intended population of predominantly non-frontal, propagating convective systems.

~~The secondary maximum of rejected frontal systems observed over the Balkans and~~ A cohesive region of frequently rejected systems extends from the eastern Alps southward along the Croatian coast and into the Balkans (Fig. 4c), highlights another important regional interaction. This area is known for significant thunderstorm activity, particularly in late summer and autumn (Galanaki et al., 2018). This activity is often linked to the interaction of synoptic systems with the Dinaric Alps and Adriatic regions (Mikuš et al., 2012). The interaction is enhanced by abundant low-level moisture and instability supplied by the warm Adriatic Sea during this period (Stocchi and Davolio, 2016). While these interactions can produce large, long-lasting precipitation systems (as noted by Galanaki et al. (2018) regarding thunderstorm size and duration over the Adriatic) that trigger our initial detection, their formation mechanism is tied to synoptic and orographic forcing, not self-sustaining mesoscale dynamics. Therefore, their removal by our filters, confirmed by their frequent association with fronts in Fig. 4d, is physically appropriate for isolating ~~genuine~~ distinct MCSs (see Fig. A1a for an example of a rejected quasi-stationary orographic system).

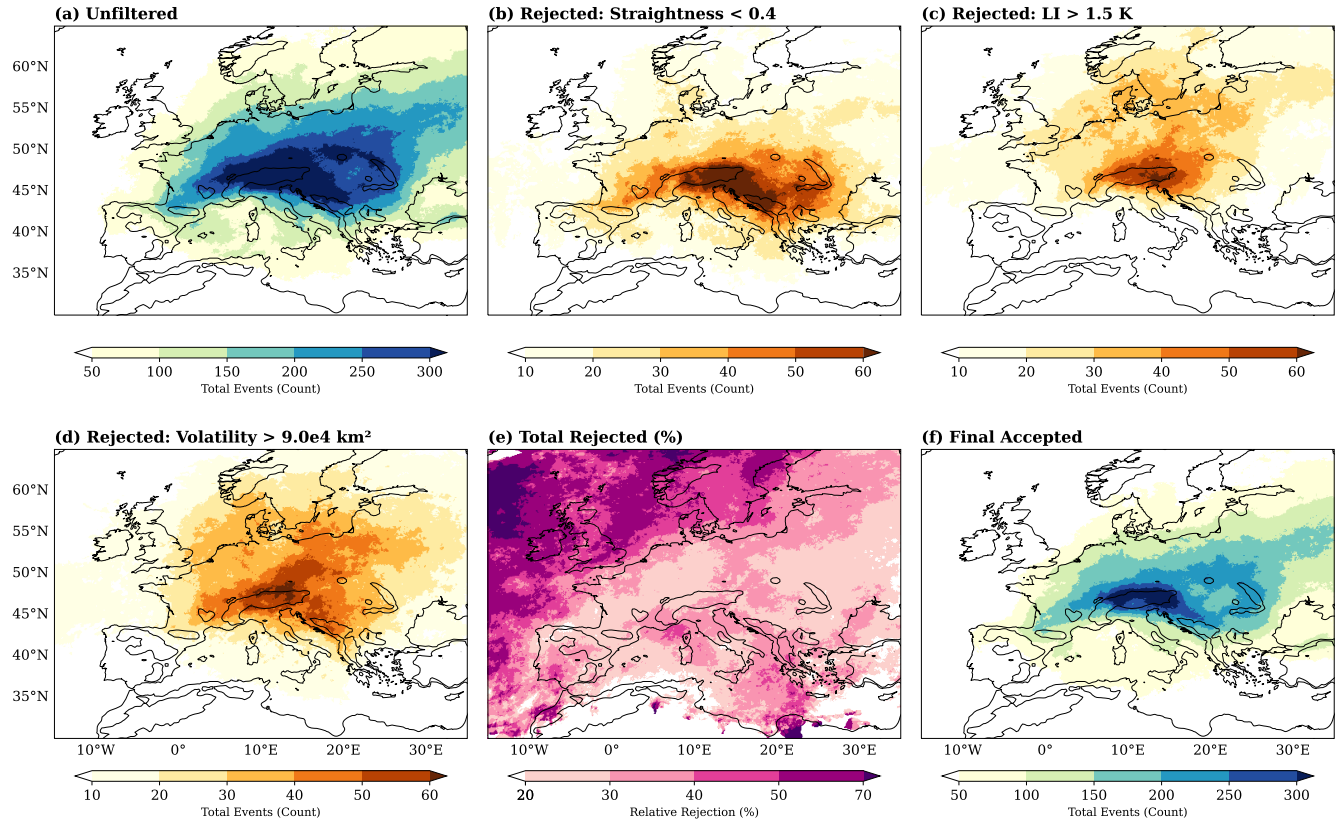

Figure 3. Spatial impact of the postprocessing filters on the MCS climatology for the warm season (May–September, 1998–2024). Maps show the total count of identified systems per grid cell. (a) Unfiltered climatology from the raw tracking output. (b–d) Systems rejected solely by the (b) track straightness, (c) mean LI, and (d) area volatility filters, respectively. Panel (e) ~~Total count~~ highlights the relative amount of ~~systems~~ total rejected ~~by any of the three filters combined~~events. (f) Final, filtered MCS climatology. Black contours indicate surface elevation above 800 m.

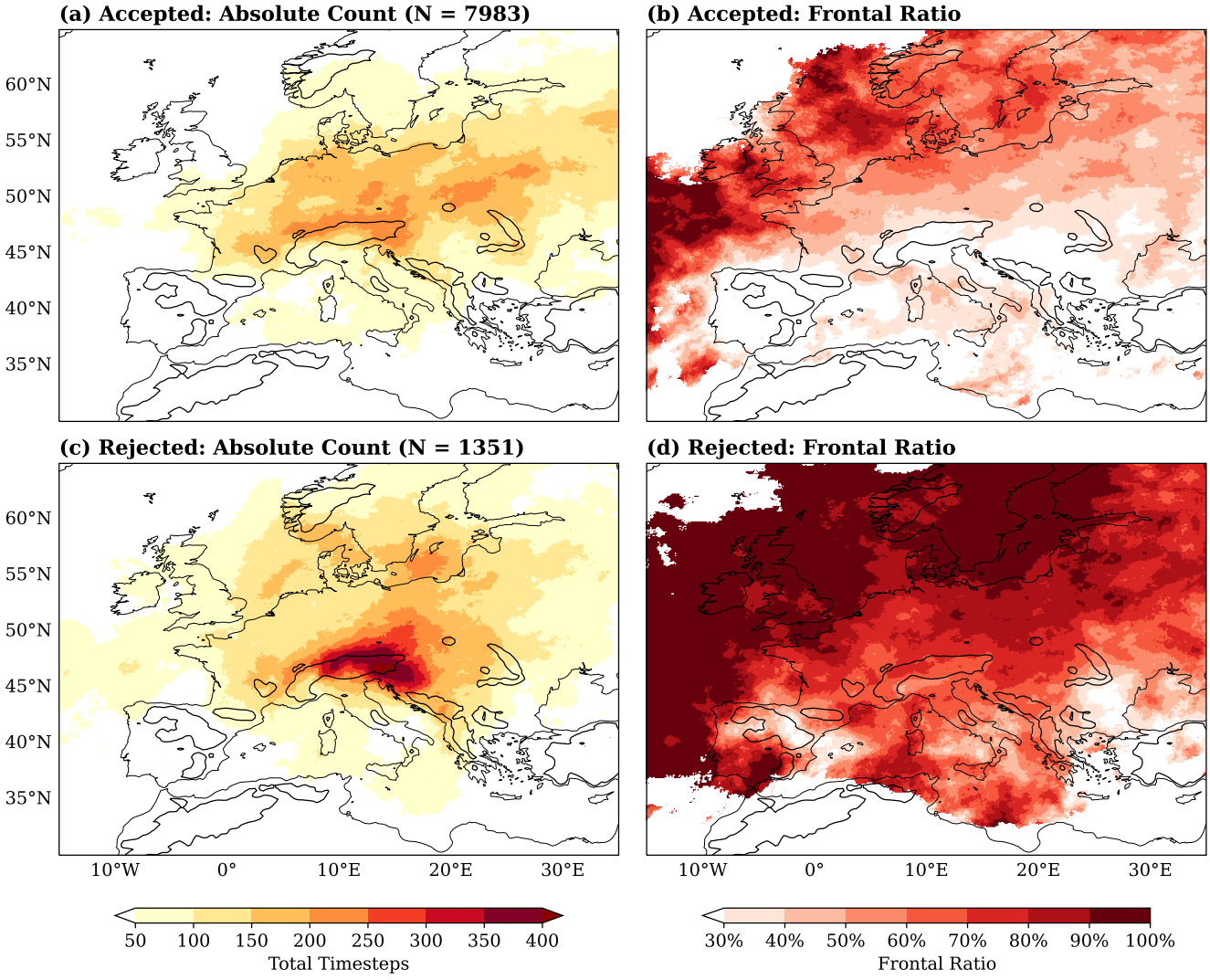

Figure 4. Validation of postprocessing filters using an independent frontal analysis (Schaffer et al., 2024) for the period 1998–2020. (a) Absolute count of hourly timesteps per grid cell where a rejected system overlapped with a detected front. (b) Ratio of frontal timesteps (panel a) to the ~~total~~ relative number of rejected timesteps per grid cell (from Fig. 3e). Grid cells with fewer than 20 total rejected timesteps are masked in panel (b) and (d). Black contours indicate surface elevation above 800 m.

4 Climatology over Europe

4.1 Spatial Distribution and Seasonal Cycle

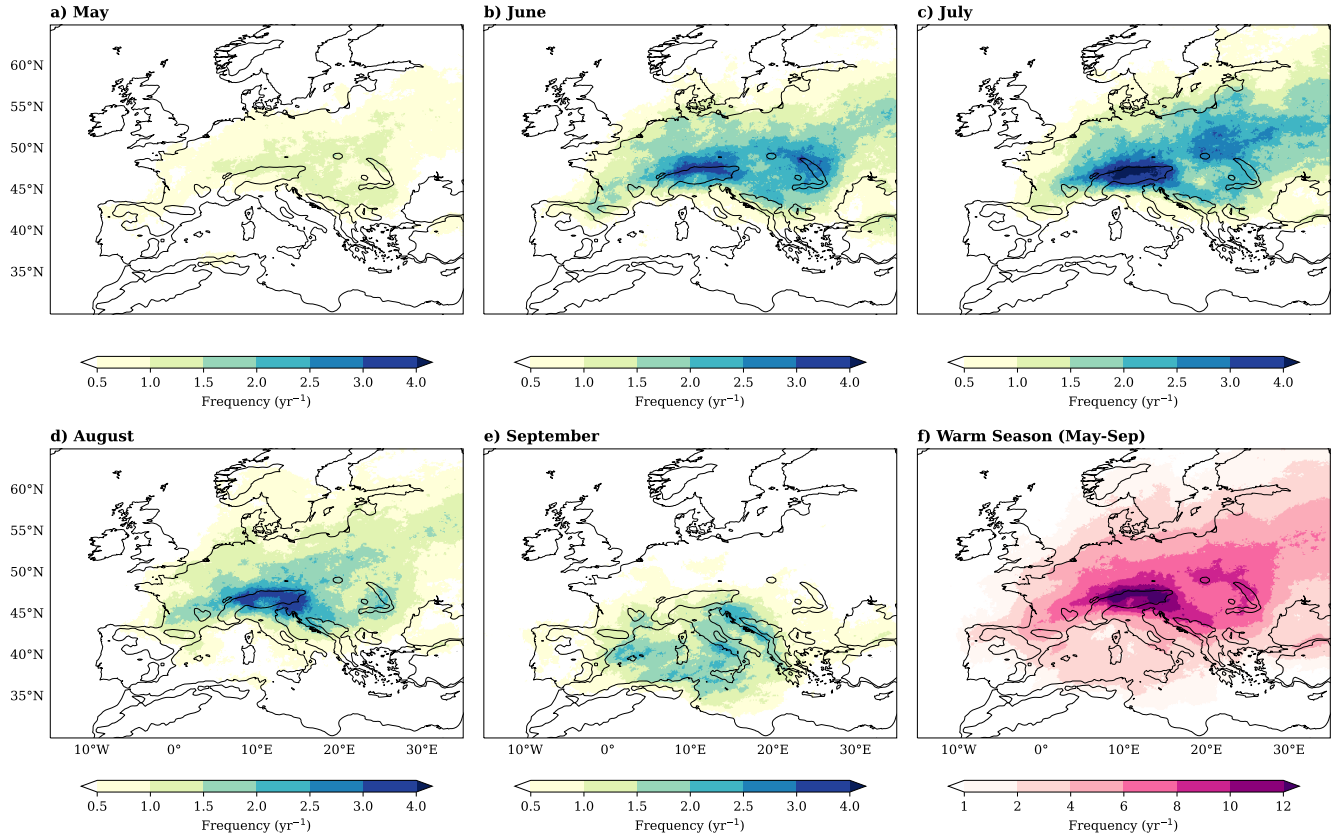

Figure 5. Climatology of ~~Mesoscale Convective Systems~~ mesoscale convective systems over Europe 1998–2024. (a–e) Averaged number of MCSs per year by month. (f) Averaged number of MCSs for the full warm season from May to September. Black contours indicate surface elevation above 800 m.

The spatial distribution and seasonal evolution of MCS frequency across Europe, derived from the 27-year EMMA-Tracker climatology (1998-2024), are presented in Fig. 5. The frequency represents the count of unique MCS overlapping each grid point during their lifetime. The overall warm season pattern (May-Sep, Fig. 5f) highlights that MCS activity is predominantly continental and strongly linked to major European mountain ranges. The most pronounced hotspots, with peak frequencies reaching over eight events per year, occur over the Alps and the Dinaric Alps/Balkan region. Secondary maxima are evident near the Massif Central, and the northern Carpathians. This strong orographic correlation , with frequency peaks often adjacent to or slightly downstream of the highest elevations, suggests propagating systems potentially initiated by orography. Regions like the British Isles, Scandinavia, and most ocean areas show minimal MCS activity.

The seasonal progression reveals a distinct geographical evolution throughout the warm months. In May (Fig. 5 a), activity ~~is relatively widespread over the continent, with maxima~~ remains relatively widespread across the continent. While scattered systems emerge over eastern France (e.g., Vosges region), the northern Carpathians, and the Balkans, ~~though counts are lower than in~~ overall frequencies remain much lower than during peak summer. By June (Fig. 5 b), the peak shifts, with the Alps and the Carpathians emerging as primary centers. Increased frequency is also noted east of the Dinaric Alps, and the Pyrenees appear to reach their peak. July (Fig. 5 c) is the overall peak month, dominated by intense activity over the Alps (both north and south sides) and over Poland. In August (Fig. 5 d), a southwestward shift occurs , with Alpine activity concentrating more westward (e.g., Lombard lakes region, eastern Alps/Slovenia and Friuli) , and activity near the Pyrenees and Massif Central and the Balkan region remaining notable. September (Fig. 5 e) marks a clear transition: continental activity wanes near the mountains, while relative frequency increases over maritime and coastal areas, particularly the Mediterranean and the Adriatic coast (e.g., Croatia).

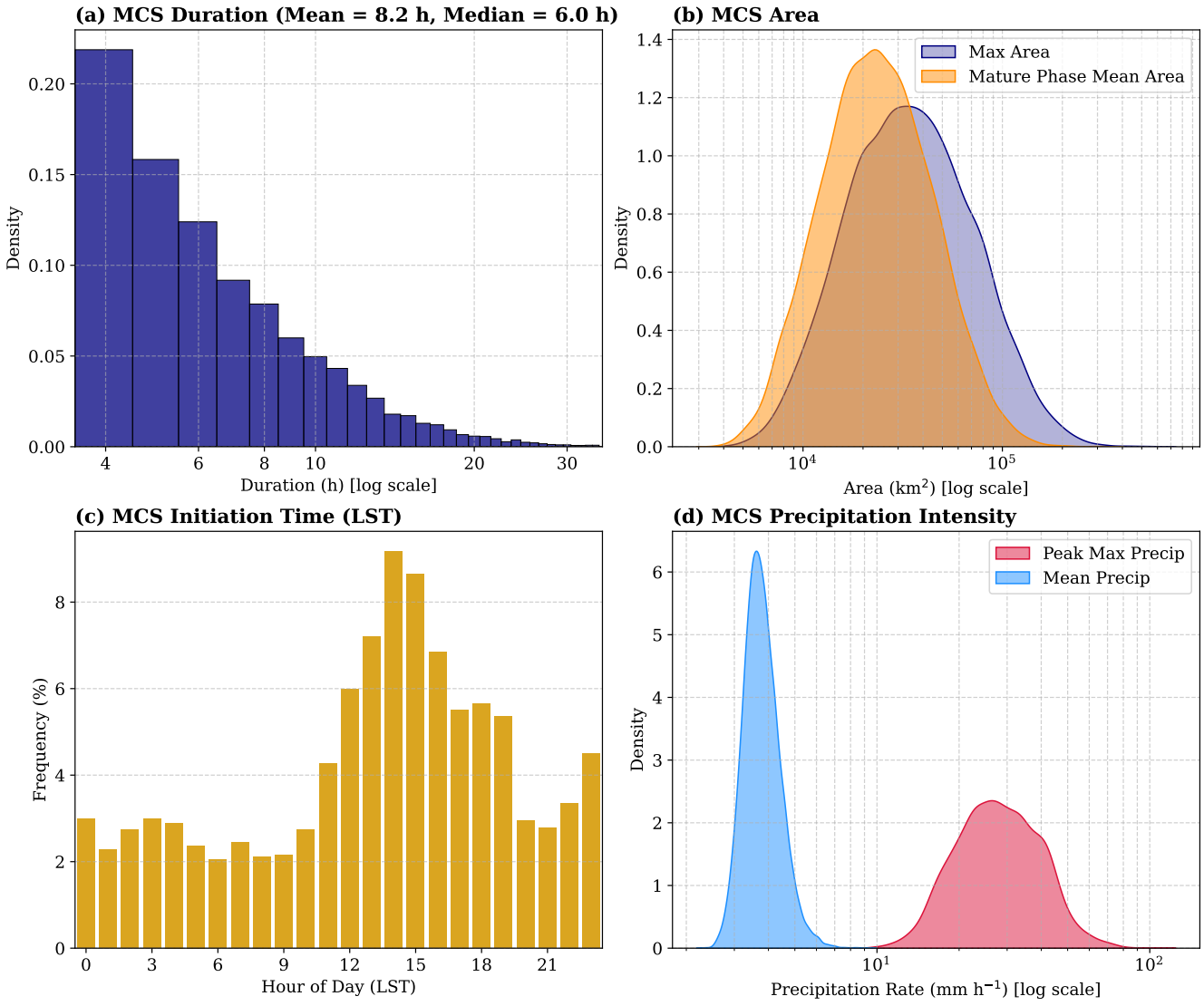

Figure 6. Distribution of MCS characteristics (May–September, 1998–2024). (a) Lifetime duration (hours). (b) Lifetime mean area and maximum area (km^2). (c) Initiation time (Local Solar Time, LST). (d) Lifetime mean precipitation intensity and track peak hourly precipitation intensity (mm h^{-1}).

Fig. 6 provides insights into the typical characteristics of the MCS population during the warm season (May-September). The distribution of MCS duration (Fig. 6a) shows a pronounced peak coinciding with the algorithm's minimum lifetime threshold of four hours, followed by a strong decrease. While the majority of systems are relatively short-lived (less than 10 hours), a notable fraction persists for well over 10 hours, indicating the presence of long-lasting convective events within the dataset. The calculated mean and median duration of 8.2 and 6 hours respectively, aligns with other European studies targeting organized MCSs (Rigo et al., 2019; Morel and Senesi, 2002) distinguishing them from the much shorter lifetimes characteristic of individual summer thunderstorms, which are usually about 35 minutes in summer according to Galanaki et al. (2018).

The distributions related to system area, based on the 1 $\mathrm{mm\,h^{-1}}$ precipitation contour, are shown in Fig. 6b. The maximum area attained by each MCS typically ranges between 10^4 and 10^5 $\mathrm{km^2}$, with a distinct mode around 30,000–40,000 $\mathrm{km^2}$. The lifetime mean area distribution of the mature phase is shifted towards smaller values, centered around 20,000–30,000 $\mathrm{km^2}$.

The diurnal cycle of MCS initiation (Fig. 6c), plotted in local solar time (LST), exhibits a distinct and dominant peak in the afternoon. Activity rises sharply from late morning, peaks strongly around 14:00 LST, and declines rapidly thereafter. This timing is consistent with convection driven by maximum solar heating and often initiated near orographic features. Some studies using different detection criteria report slightly later maxima (Da Silva and Haerter, 2023). EMMA-Tracker earlier initiation peak may reflect its ability to track systems from earlier stages, potentially capturing the upscale growth phase from organized thunderstorms into mature MCSs. Nocturnal initiations are considerably less frequent, although a slight secondary increase is noticeable around midnight LST. This nocturnal activity could be linked to the propagation of systems initiated earlier, nocturnal low-level jet dynamics, or other mesoscale forcing mechanisms independent of diurnal heating (Morel and Senesi, 2002; Da Silva and Haerter, 2023).

Finally, the precipitation intensity distributions (Fig. 6d) highlight the difference between sustained and peak rainfall within MCSs. The lifetime mean precipitation rate across all identified MCS tracks is typically low, clustering tightly around 3-4 $\mathrm{mm\,h^{-1}}$. In contrast, the distribution of the highest single hourly precipitation rate observed anywhere within each MCS track is notably broader, peaking around 20-30 $\mathrm{mm\,h^{-1}}$ but extending to values exceeding 70 $\mathrm{mm\,h^{-1}}$.

~~Although a detailed mechanistic analysis is beyond the scope of this study and warrants~~ Together, the spatial distribution (Fig. 5) and system properties (Fig. 6) demonstrate that the EMMA-climatology reflects the primary physical drivers of European convection. While a deeper study of these mechanisms is left for future investigation, the ~~climatology reflects key physical controls. The strong terrain association points to orographic lifting , the summer continental peak aligns with maximum~~ results align with established physical controls, such as orographic lifting near major mountain ranges, solar heating driving instability over the continent in summer, and the ~~September shift towards maritime regions reflects the~~ influence of the ~~relatively~~ warm Mediterranean Sea during the September maritime shift. The identification of these orographic hotspots, the clear summer continental peak, and the autumn-ward shift to the Mediterranean confirms that the EMMA-Tracker captures the fundamental, well-established drivers of European convection, aligning with the findings of numerous satellite, radar, and lightning-based studies (Morel and Senesi, 2002; Da Silva and Haerter, 2023; Galanaki et al., 2018; Rigo et al., 2019; Taszarek et al., 2019). This refined climatology of ~~propagating, non-frontally dominated~~ distinct MCSs provides a ~~distinct benchmark for process-based~~ robust benchmark for the process-oriented evaluation of organized convection in climate models.

4.2 MCSs are the strongest contributor to warm season hourly heavy precipitation

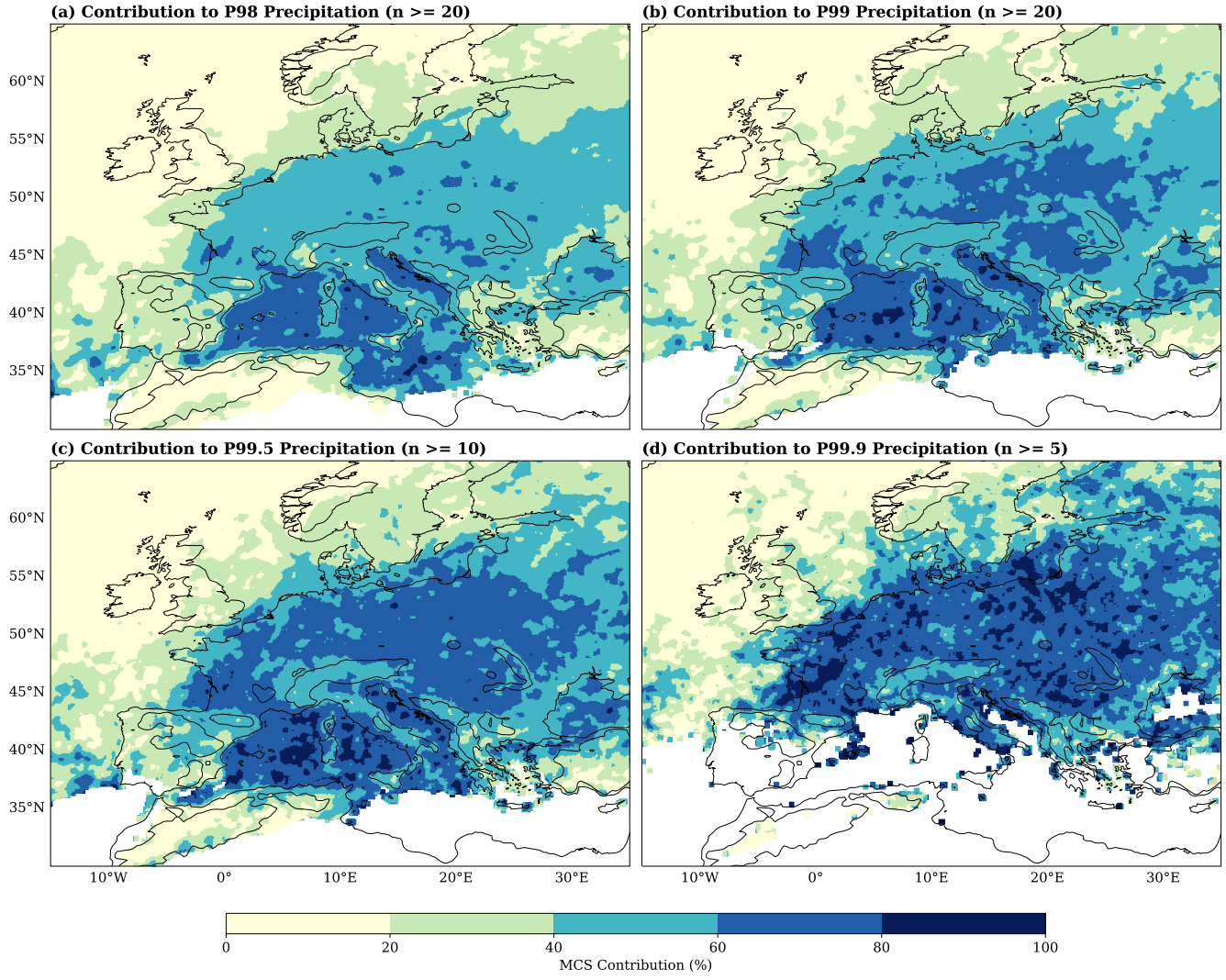

Figure 7. MCS contribution (in %) to heavy hourly precipitation for the warm season (May–September, 1998–2024). Panels show the contribution to events exceeding the pixel-wise (a) 98th, (b) 99th, (c) 99.5th, and (d) 99.9th percentile of wet hourly precipitation (hours $>$ 0.1 $\mathrm{mm\,h^{-1}}$). The maps are smoothed using a 5-pixel rolling mean for visualization. Grid cells with a low number n of total hourly events in the respective percentile are masked. Black contours indicate surface elevation above 800 m.

While the contribution of MCSs warm-season precipitation sum is moderate, generally 10-30% in continental hotspots (Fig. S5; (Da Silva and Haerter, 2023)), a starkly different picture emerges for heavy hourly precipitation events.

Fig. 7 illustrates the percentage contribution of identified MCSs to hourly precipitation, binned by increasing intensity. These percentiles (P98, P99, P99.5, P99.9) are calculated pixel-wise from the distribution of wet hours (> 0.1 $\mathrm{mm\,h^{-1}}$) for the 1998-2024 warm season. The local return period of these events also depends on the local ~~Wet Hour Frequency~~ wet hour frequency (WHF, Fig. S6).

A clear pattern is evident across continental Europe: the relative contribution of these systems as a driver of hourly precipitation systematically increases with the intensity of the event. For the 98th percentile (Fig. 7a), MCSs already account for a substantial portion (40-60%) of precipitation over most of continental Europe and the Mediterranean. This contribution becomes dominant for P99.5 events (Fig. 7c) and is highest for the P99.9 percentile (Fig. 7d).

However, this continental pattern is bounded by two distinct regimes. First, consistent with the filter validation (Fig. 4), there is a notable absence of substantial MCS contribution over the North Atlantic storm track. Second, a different pattern emerges over the high-elevation orographic hotspots. In contrast to the surrounding plains, the relative MCS contribution is visibly lower directly over the core of major mountain ranges, such as the Alps, Dinaric Alps, and Carpathians (Fig. 7b). This pattern persists even for the highest P99.9 percentile (Fig. 7d), where contributions over the high Alps remain in the 40–60% range, while surrounding plains in France, Germany, and the Po Valley reach values up to 80%. This suggests that frequent, localized (and potentially quasi-stationary orographic) thunderstorms, are also a substantial contributor to even the most intense hourly precipitation events in these specific, high-elevation thunderstorm hotspots.

4.3 Limitations and Recommendations for Usage

The EMMA-Tracker and the resulting climatology dataset have ~~several~~ some important conceptual limitations, stemming from both the input data and the algorithm's specific scientific goals. These limitations also inform the recommended best practices for its primary application: climatological studies and climate model evaluation. It has to be mentioned at this point that this dataset is not a meteorological record and systems for meteorological case studies should be carefully investigated in the specific cases.

Tracking MCSs using only precipitation can artificially split systems and prematurely terminate their lifecycles, because precipitation beneath a continuous convective cloud shield is often patchy and spatially discontinuous (Fiolleau and Roca, 2013; Feng et al., . Recent hybrid trackers overcome this by incorporating infrared brightness temperatures or simulated outgoing longwave radiation (OLR) to follow the continuous upper-level cloud canopy (Feng et al., 2021a). However, this approach requires hourly OLR, which is rarely available in standard regional climate model output due to data storage constraints. Despite this limitation, precipitation has a high socioeconomically relevance for assessing convective impacts. To mitigate track splitting within discontinuous precipitation, our method uses a low initial threshold (1 mm $\mathrm{h^{-1}}$), applies spatial smoothing to connect fragmented cores, and utilizes a temporal recovery strategy to bridge short gaps (Moseley et al., 2013).

A fundamental aspect of the EMMA-Tracker is its specific conceptual definition of an MCS. The post-processing filters are a deliberate methodological choice to isolate a robust set of ~~propagating, self-sustaining, non-frontal-dominated systems~~

systems that maintain a clear shape and steady movement, remaining structurally distinct from any co-occurring synoptic triggers. The straightness filter (Fig. A1a) effectively removes quasi-stationary systems over orography, which, as the analysis of heavy precipitation suggests (Fig. 7), are likely a major contributor to heavy rain in high-alpine regions but are conceptually distinct from the propagating different from the distinct MCSs targeted here. Furthermore, while the filters are highly effective at removing synoptic-scale fronts (Fig. 4), this process may also exclude some genuine squall lines embedded in fronts if their precipitation field is artificially merged embedded with the larger front frontal precipitation in the $0.1°$ IMERG data at some point.

The methodology is also constrained by its input data. The algorithm's performance depends on precipitation data that can adequately resolve the morphology of convective plumes (Fig. S3S1). While the $0.1°$ IMERG resolution is sufficient, the tracker is not suitable for coarse-resolution General Circulation Models (GCMs), where an MCS would be the size of only a few grid cells.

A further limitation stems from deriving the atmospheric instability proxy (Lifted Index) from ERA5, which relies on parameterized convection and may not perfectly align spatiotemporally with the explicitly observed IMERG precipitation. We do not intend to use this proxy as a quantitative predictor of precipitation intensity, but rather as an effective qualitative threshold to identify environments broadly supportive of convection. Furthermore, this observational mismatch is naturally avoided when applying the algorithm to climate model data, since simulated precipitation is a direct consequence of the model's own representation of atmospheric instability.

The use of $0.25°$ ERA5 data for the LI introduces a resolution mismatch. This is considered a minor limitation, as the LI is a relatively smooth field and the criteria for its use (10% overlap for one timestep) are not overly restrictive for systems with a minimum size of 3500 km^2. Finally, this study is restricted to the warm season (May-September). The prevalence of frontal systems relative to MCSs increases substantially in the cold season over Europe. This dominance of synoptically-driven precipitation makes the application of this specific filter set unreliable for isolating MCSs during winter monthsMay–September). In winter, European weather is so dominated by synoptic fronts that any attempt to track rare MCSs would result in a dataset overwhelmed by frontal false positives.

For the intended purpose of model evaluation, these limitations provide clear guidance. The algorithm's sensitivity to precipitation morphology makes direct comparisons between different datasets (e.g., observations vs. model, or RCM vs. CPM) susceptible to detection biases. To ensure a fair and physically meaningful comparison, all datasets should first be remapped to a common grid (e.g., the 12.5 km EURO-CORDEX grid when comparing an 12.5 km RCM with a 3 km CPM) before applying the tracker. This isolates the models ability to produce organized systems from the simple fact that higher-resolution data resolves smaller features. While the EMMA-Tracker can be applied to native high-resolution model output, the results are not directly comparable to this climatology on the IMERG grid unless morphology-dependent parameters are recalibrated. Most climate model ensembles, such as EURO-CORDEXhave , only provide the pressure level data , needed for the LI calculation, only available at six hourly temporal needed for LI calculations at a six-hourly resolution (EURO-CORDEX, 2022). Which This requires interpolation to match the hourly precipitation data. Another point worth mentioning is the use of lower temporal resolution data, while it is in general possible with Sensitivity tests suggest that the tracker can still effectively identify MCSs

with this temporal mismatch, as the LI filter is designed to be a broad environmental constraint rather than a precise predictor of convective activity (not shown). Additionally, while the EMMA-Tracker ~~, but~~ can generally handle lower temporal resolution data, its suitability should be evaluated ~~in the according cases~~on a case-by-case basis.

5 Conclusions

In this study, we presented the EMMA-Tracker, a novel algorithm specifically designed to identify and track ~~Mesoscale Convective Systems~~ mesoscale convective systems (MCSs) using only variables available in standard climate model output. A key innovation of this method is the application of physics-based filters that utilize the system's full spatiotemporal lifecycle, allowing for a robust separation of propagating MCSs from synoptically-driven or stationary precipitation features. We applied this tracker to IMERG precipitation and ~~IMERG~~ ERA5 data to generate a 27-year (1998–2024) warm-season climatology, representing the longest such dataset for Europe to date.

The final climatology shows that MCS activity is predominantly continental during summer, with the highest frequencies concentrated near major mountain ranges, particularly the Alps, Dinaric Alps. In September, a clear transition occurs as activity wanes over the continent and shifts toward maritime and coastal regions, especially the Mediterranean and Adriatic Seas. We could show that MCS are the most dominant source of heavy hourly precipitation (P99.9) over most of continental Europe.

This dataset is not only restricted for model evaluation but itself represents a robust observational record that enables in-depth climatological analysis of organized convection over Europe. Beyond climatological comparisons, the dataset is designed for process-based evaluation of European climate model ensembles, such as EURO-CORDEX and FPS-CONV. By providing the exact time and location of propagating systems, the EMMA-Tracker allows researchers to move beyond simple bias maps and investigate the physical drivers of convection–such as moisture flux, vertical wind shear, and cold pool strength—throughout the MCS lifecycle. This capability is essential for estimating the uncertainties in future climate projections and for understanding how these high-impact systems will evolve in a warming world. Ultimately, improving our ability to model these systems is a prerequisite for effective disaster preparedness and adaptation to future hydrological hazards.

~~While this study focused on the European domain, the physics-based principles of the EMMA-Tracker are transferable. With appropriate calibration of the filtering thresholds to local environmental conditions, this methodology can be applied to other regions, offering a pathway toward a globally consistent framework for evaluating organized~~

Code and data availability. The EMMA-Tracker v1.0 software used in this study to identify and track systems is permanently archived on Zenodo at https://doi.org/10.5281/zenodo.19233057, with the active development repository available on GitHub (https://github.com/DavidKneidinger/emma-tracker/). The specific analysis scripts utilized for this manuscript are permanently archived at https://doi.org/10.5281/zenodo.19234249. The resulting gridded MCS masks of the 27-year European MCS climatology (1998–2024) generated in this study is available on Zenodo (https://doi.org/10.5281/zenodo.18234275; Kneidinger, 2026).

The original input datasets are provided by the NASA Goddard Earth Sciences Data and Information Services Center (GES DISC) for GPM IMERG Final Precipitation L3 Half Hourly V07 (https://doi.org/10.5067/GPM/IMERG/3B-HH/07) and the Copernicus Climate

Change Service (C3S) Climate Data Store (CDS) for ERA5 hourly data on single levels (https://doi.org/10.24381/cds.adbb2d47) and pressure levels (https://doi.org/10.24381/cds.bd0915c6). To ensure strict long-term data preservation and reproducibility, the exact subsets of these raw input datasets utilized in this study have been permanently archived on Zenodo. ERA5 pressure level data for 1998–2010 (https://doi.org/10.5281/zenodo.19347622), ERA5 pressure level data for 2011–2024 (https://doi.org/10.5281/zenodo.19347730), and combined ERA5 surface and IMERG precipitation data for 1998–2024 (https://doi.org/10.5281/zenodo.19347740).

Appendix A: Postprocessing Filter Examples

This section shows examples of systems that can be removed by the individual postprocessing filters.

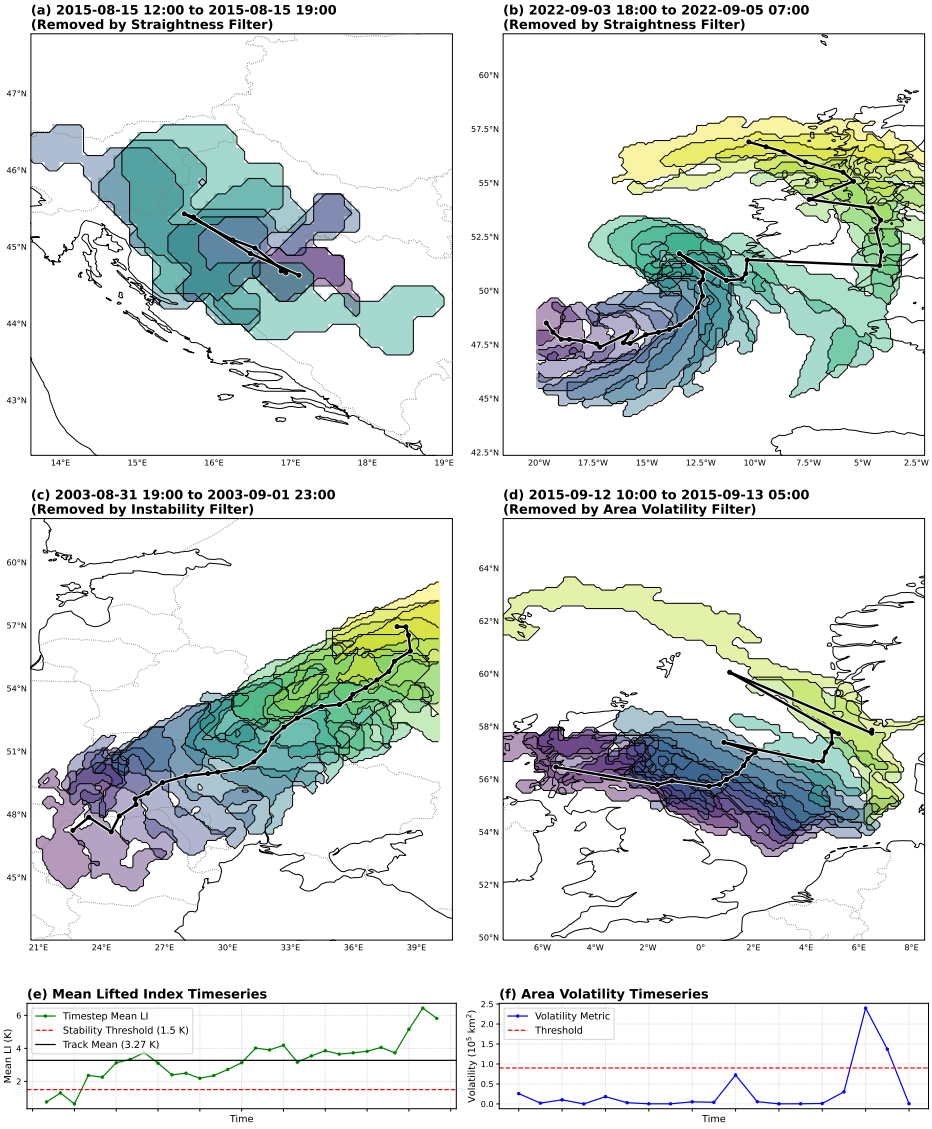

Figure A1. Examples of tracks identified by the initial detection algorithm but subsequently removed by the postprocessing filters. The colored lines show the path of the precipitation-weighted centroid for each hour of the track's life ranging from purple (first detection) to yellow (last detection). (a) A quasi-stationary system over the Dinaric Alps rejected by the straightness filter due to its erratic, non-propagating movement. (b) A large, slow-moving synoptic frontal system over the North Atlantic, also rejected by the straightness filter because its centroid shifted erratically as embedded precipitation cells evolved. (c) A long-lived frontal system rejected by the environmental instability filter. The corresponding time series in (e) shows its mean Lifted Index (LI) over the track was 3.27 K, indicating it existed in an on-average highly stable environment. (d) A system over northern Europe rejected by the area volatility filter. The corresponding time series in (f) shows a physically implausible spike in volatility, characteristic of the algorithm erroneously merging a separate, nearby precipitation system.

Author contributions. DK developed the EMMA-Tracker algorithm , performed the 27-year climatological analysis, and generated the resulting European MCS dataset. DK created all visualizations and wrote the original manuscript draft. AS curated and provided the independent frontal database used for the filter validation and analysis of frontal precipitation contributions. DM provided scientific supervision and guidance throughout the study. All authors contributed to the review and editing of the final manuscript.

Competing interests. The authors declare to not have any competing interests.

Acknowledgements. This research was funded by the Austrian Research Promotion Agency (FFG) within the "MoCCA" project (Mesoscale convective systems under Climate Change over the Alps) (913124). We gratefully acknowledge our project partners at GeoSphere Austria, specifically Klaus Haslinger and Benedikt Bica and Georg Pistotnik for their valuable discussions, and for providing meteorological expertise and a list of reference systems that were essential during the development phase. We thank Zhe Feng for providing the PyFLEXTRKR MCS dataset which served as a helpful reference during algorithm development. We extend our gratitude to our colleagues at the Wegener Center, with special thanks to Heimo Truhetz for his ongoing support and constructive scientific discussions.

References

Ban, N., Caillaud, C., Coppola, E., Pichelli, E., Sobolowski, S., Adinolfi, M., Ahrens, B., Alias, A., Anders, I., Bastin, S., et al.: The first multi-model ensemble of convection-permitting simulations of European climate, Climate Dynamics, 57, 369–394, 2021.

Berg, P., Moseley, C., and Haerter, J. O.: Strong increase in convective precipitation in response to higher temperatures, Nature Geoscience, 6, 181–185, 2013.

Catto, J. L. and Pfahl, S.: The importance of fronts for extreme precipitation, Journal of Geophysical Research: Atmospheres, 118, 10–791, 2013.

Catto, J. L., Nicholls, N., Jakob, C., and Shelton, K. L.: Atmospheric fronts in current and future climates, Geophysical Research Letters, 41, 7642–7650, https://doi.org/https://doi.org/10.1002/2014GL061943, 2014.

Coppola, E., Sobolowski, S., Pichelli, E., Raffaele, F., Ahrens, B., Anders, I., Ban, N., Bastin, S., Belda, M., Belusic, D., et al.: A first-of-its-kind multi-model convection permitting ensemble for investigating convective phenomena over Europe and the Mediterranean, Climate Dynamics, 55, 3–34, 2020.

Cui, W., Dong, X., Xi, B., Feng, Z., and Fan, J.: Can the GPM IMERG Final Product Accurately Represent MCSs' Precipitation Characteristics over the Central and Eastern United States?, Journal of Hydrometeorology, 21, 39 – 57, https://doi.org/10.1175/JHM-D-19-0123.1, 2020.

Cui, W., Galarneau Jr., T. J., and Hoogewind, K. A.: Changes in Mesoscale Convective System Precipitation Structures in Response to a Warming Climate, Journal of Geophysical Research: Atmospheres, 129, e2023JD039 920, https://doi.org/https://doi.org/10.1029/2023JD039920, e2023JD039920 2023JD039920, 2024.

Da Silva, N. A. and Haerter, J. O.: The Precipitation Characteristics of Mesoscale Convective Systems Over Europe, Journal of Geophysical Research: Atmospheres, 128, e2023JD039 045, https://doi.org/https://doi.org/10.1029/2023JD039045, e2023JD039045 2023JD039045, 2023.

Doblas-Reyes, F., Sörensson, A., Almazroui, M., Dosio, A., Gutowski, W., Haarsma, R., Hamdi, R., Hewitson, B., Kwon, W.-T., Lamptey, B., Maraun, D., Stephenson, T., Takayabu, I., Terray, L., Turner, A., and Zuo, Z.: IPCC AR6 WGI Chapter 10: Linking global to regional climate change, pp. 1363–1512, ISBN 9781009157896, https://doi.org/10.1017/9781009157896.012, 2021.

Dong, B., Sutton, R. T., Woollings, T., and Hodges, K.: Variability of the North Atlantic summer storm track: mechanisms and impacts on European climate, Environmental Research Letters, 8, 034 037, 2013.

Dougherty, E. M., Prein, A. F., Gutmann, E. D., and Newman, A. J.: Future Simulated Changes in Central U.S. Mesoscale Convective System Rainfall Caused by Changes in Convective and Stratiform Structure, Journal of Geophysical Research: Atmospheres, 128, e2022JD037 537, https://doi.org/https://doi.org/10.1029/2022JD037537, e2022JD037537 2022JD037537, 2023.

EURO-CORDEX: EURO-CORDEX-CMIP6 Atmosphere Variable List, https://doi.org/10.5281/zenodo.8414798, 2022.

Eyring, V., Cox, P. M., Flato, G. M., Gleckler, P. J., Abramowitz, G., Caldwell, P., Collins, W. D., Gier, B.-M., Hall, A. D., Hoffman, F. M., et al.: Taking climate model evaluation to the next level, Nature Climate Change, 9, 102–110, 2019.

Feng, Z., Leung, L. R., Liu, N., Wang, J., Houze Jr, R. A., Li, J., Hardin, J. C., Chen, D., and Guo, J.: A Global High-Resolution Mesoscale Convective System Database Using Satellite-Derived Cloud Tops, Surface Precipitation, and Tracking, Journal of Geophysical Research: Atmospheres, 126, e2020JD034 202, https://doi.org/https://doi.org/10.1029/2020JD034202, e2020JD034202 2020JD034202, 2021a.

Feng, Z., Song, F., Sakaguchi, K., and Leung, L. R.: Evaluation of Mesoscale Convective Systems in Climate Simulations: Methodological Development and Results from MPAS-CAM over the United States, Journal of Climate, 34, 2611 – 2633, https://doi.org/10.1175/JCLI-D-20-0136.1, 2021b.

Feng, Z., Hardin, J., Barnes, H. C., Li, J., Leung, L. R., Varble, A., and Zhang, Z.: PyFLEXTRKR: a flexible feature tracking Python software for convective cloud analysis, Geoscientific Model Development, 16, 2753–2776, https://doi.org/10.5194/gmd-16-2753-2023, 2023.

Feng, Z., Prein, A. F., Kukulies, J., Fiolleau, T., Jones, W. K., Maybee, B., Moon, Z. L., Núñez Ocasio, K. M., Dong, W., Molina, M. J., Albright, M. G., Rajagopal, M., Robledo, V., Song, J., Song, F., Leung, L. R., Varble, A. C., Klein, C., Roca, R., Feng, R., and Mejia, J. F.: Mesoscale Convective Systems Tracking Method Intercomparison (MCSMIP): Application to DYAMOND Global km-Scale Simulations, Journal of Geophysical Research: Atmospheres, 130, e2024JD042 204, https://doi.org/https://doi.org/10.1029/2024JD042204, e2024JD042204 2024JD042204, 2025.

Fery, L. and Faranda, D.: Analysing 23 years of warm-season derechos in France: a climatology and investigation of synoptic and environmental changes, Weather and Climate Dynamics, 5, 439–461, https://doi.org/10.5194/wcd-5-439-2024, 2024.

Fiolleau, T. and Roca, R.: A new methodology for the detection and tracking of mesoscale convective systems in the tropics using geostationary infrared data, Journal of Applied Meteorology and Climatology, 52, 1327–1344, 2013.

Fosser, G., Khodayar, S., and Berg, P.: The effect of resolution and convection-permitting climate modeling on future precipitation change in the Alps, Journal of Climate, 28, 6187–6203, 2015.

Galanaki, E., Lagouvardos, K., Kotroni, V., Flaounas, E., and Argiriou, A.: Thunderstorm climatology in the Mediterranean using cloud-to-ground lightning observations, Atmospheric Research, 207, 136–144, 2018.

García-Herrera, R., Hernández, E., Paredes, D., Barriopedro, D., Correoso, J., and Prieto, L.: A MASCOTTE-based characterization of MCSs over Spain, 2000–2002, Atmospheric Research, 73, 261–282, https://doi.org/https://doi.org/10.1016/j.atmosres.2004.11.003, 2005.

Gatzen, C. and Pucik, T.: Analysis of the high-end derecho in Corsica in 2022, in: ECSS 2023 - 12th European Conference on Severe Storms, https://meetingorganizer.copernicus.org/ECSS2023/ECSS2023-148.html, 2023.

Haberlie, A. M. and Ashley, W. S.: Climatological representation of mesoscale convective systems in a dynamically downscaled climate simulation, International Journal of Climatology, 39, 1144–1153, https://doi.org/https://doi.org/10.1002/joc.5880, 2019.

Haslinger, K., Breinl, K., Pavlin, L., Pistotnik, G., Bertola, M., Olefs, M., Greilinger, M., Schöner, W., and Blöschl, G.: Increasing hourly heavy rainfall in Austria reflected in flood changes, Nature, 639, 667–672, 2025.

Hayden, L., Liu, C., and Liu, N.: Properties of Mesoscale Convective Systems Throughout Their Lifetimes Using IMERG, GPM, WWLLN, and a Simplified Tracking Algorithm, Journal of Geophysical Research: Atmospheres, 126, e2021JD035 264, https://doi.org/https://doi.org/10.1029/2021JD035264, e2021JD035264 2021JD035264, 2021.

Hersbach, H., Bell, B., Berrisford, P., Biavati, G., Horányi, A., Muñoz Sabater, J., Nicolas, J., Peubey, C., Radu, R., Rozum, I., Schepers, D., Simmons, A., Soci, C., Dee, D., and Thépaut, J.-N.: ERA5 hourly data on single levels from 1940 to present, https://doi.org/10.24381/cds.adbb2d47, [Dataset], Accessed on 31-05-2025, 2023.

Hohenegger, C., Brockhaus, P., Bretherton, C. S., and Schär, C.: An intercomparison of regional climate simulations for Europe: assessing uncertainties in model projections, Climate Dynamics, 33, 929–946, 2009.

Huffman, G. J., Stocker, E. F., Bolvin, D. T., Nelkin, E. J., and Tan, J.: GPM IMERG final precipitation l3 hourly 0.1 degree x 0.1 degree v07, https://doi.org/10.5067/GPM/IMERG/3B-HH/07, [Dataset], Accessed on 17-07-2025, 2019.

Hénin, R., Ramos, A. M., Schemm, S., Gouveia, C. M., and Liberato, M. L. R.: Assigning precipitation to mid-latitudes fronts on sub-daily scales in the North Atlantic and European sector: Climatology and trends, International Journal of Climatology, 39, 317–330, https://doi.org/https://doi.org/10.1002/joc.5808, 2019.

Jacob, D., Petersen, J., Eggert, B., Alias, A., Christensen, O. B., Bouwer, L. M., Braun, A., Colette, A., Déqué, M., Georgievski, G., et al.: EURO-CORDEX: new high-resolution climate change projections for European impact research, Regional environmental change, 14, 563–578, 2014.

Jacob, D., Teichmann, C., Sobolowski, S., Katragkou, E., Anders, I., Belda, M., Benestad, R., Boberg, F., Buonomo, E., Cardoso, R. M., et al.: Regional climate downscaling over Europe: perspectives from the EURO-CORDEX community, Regional environmental change, 20, 51, 2020.

Kendon, E. J., Ban, N., Roberts, N. M., Fowler, H. J., Roberts, M. J., Chan, S. C., Evans, J. P., Fosser, G., and Wilkinson, J. M.: Do Convection-Permitting Regional Climate Models Improve Projections of Future Precipitation Change?, Bulletin of the American Meteorological Society, 98, 79 – 93, https://doi.org/10.1175/BAMS-D-15-0004.1, 2017.

Kendon, E. J., Roberts, N. M., Senior, C. A., and Roberts, M. J.: Future changes in extreme precipitation and landslides, Climate, 9, 59, 2021.

Kolios, S. and Feidas, H.: A warm season climatology of mesoscale convective systems in the Mediterranean basin using satellite data, Theoretical and Applied Climatology, 102, 29–42, https://doi.org/10.1007/s00704-009-0241-7, 2010.

Kotlarski, S., Keuler, K., Christensen, O. B., Colette, A., Déqué, M., Gobiet, A., Goergen, K., Jacob, D., Lüthi, D., van Meijgaard, E., et al.: Regional climate modeling on European scales: a joint standard evaluation of the EURO-CORDEX RCM ensemble, Geoscientific Model Development, 7, 1297–1333, 2014.

Lin, G., Jones, C. R., Leung, L. R., Feng, Z., and Ovchinnikov, M.: Mesoscale Convective Systems in a Superparameterized E3SM Simulation at High Resolution, Journal of Advances in Modeling Earth Systems, 14, e2021MS002 660, https://doi.org/https://doi.org/10.1029/2021MS002660, e2021MS002660 2021MS002660, 2022.

Markowski, P. and Richardson, Y.: Mesoscale meteorology in midlatitudes, John Wiley & Sons, 2011.

Meredith, E. P., Ulbrich, U., and Rust, H. W.: The diurnal cycle of hourly precipitation over Germany in the CORDEX-CORE ensemble and in a convection-permitting model, Natural Hazards and Earth System Sciences, 21, 2543–2557, 2021.

Mikuš, P., Prtenjak, M. T., and Mahović, N. S.: Analysis of the convective activity and its synoptic background over Croatia, Atmospheric Research, 104, 139–153, 2012.

Mohammed, S., Nasr, A., and Mahmoud, M.: Comprehensive Assessment of GPM-IMERG and ERA5 Precipitation Products Across Ireland, Remote Sensing, 17, https://doi.org/10.3390/rs17183154, 2025.

Morel, C. and Senesi, S.: A climatology of mesoscale convective systems over Europe using satellite infrared imagery. II: Characteristics of European mesoscale convective systems, Quarterly Journal of the Royal Meteorological Society, 128, 1973–1995, https://doi.org/https://doi.org/10.1256/003590002320603494, 2002.

Moseley, C., Berg, P., and Haerter, J. O.: Probing the precipitation life cycle by iterative rain cell tracking, Journal of Geophysical Research: Atmospheres, 118, 13,361–13,370, https://doi.org/https://doi.org/10.1002/2013JD020868, 2013.

Navarro, A., García-Ortega, E., Merino, A., Sánchez, J. L., Kummerow, C., and Tapiador, F. J.: Assessment of IMERG Precipitation Estimates over Europe, Remote Sensing, 11, https://doi.org/10.3390/rs11212470, 2019.

Núñez Ocasio, K. M. and Moon, Z. L.: TAMS: a tracking, classifying, and variable-assigning algorithm for mesoscale convective systems in simulated and satellite-derived datasets, Geoscientific Model Development, 17, 6035–6049, 2024.

O, S., Foelsche, U., Kirchengast, G., Fuchsberger, J., Tan, J., and Petersen, W. A.: Evaluation of GPM IMERG Early, Late, and Final rainfall estimates using WegenerNet gauge data in southeastern Austria, Hydrology and Earth System Sciences, 21, 6559–6572, https://doi.org/10.5194/hess-21-6559-2017, 2017.

Pradhan, R. K., Markonis, Y., Vargas Godoy, M. R., Villalba-Pradas, A., Andreadis, K. M., Nikolopoulos, E. I., Papalexiou, S. M., Rahim, A., Tapiador, F. J., and Hanel, M.: Review of GPM IMERG performance: A global perspective, Remote Sensing of Environment, 268, 112 754, https://doi.org/https://doi.org/10.1016/j.rse.2021.112754, 2022.

Prein, A. F., Langhans, W., Fosser, G., Ferrone, A., Ban, N., Goergen, K., Keller, M., Tölle, M., Gutjahr, O., Feser, F., Brisson, E., Kollet, S., Schmidli, J., van Lipzig, N. P. M., and Leung, R.: A review on regional convection-permitting climate modeling: Demonstrations, prospects, and challenges, Reviews of Geophysics, 53, 323–361, https://doi.org/https://doi.org/10.1002/2014RG000475, 2015.

Prein, A. F., Liu, C., Ikeda, K., Trier, S. B., Rasmussen, R. M., Holland, G. J., and Clark, M. P.: Increased rainfall volume from future convective storms in the US, Nature Climate Change, 7, 880–884, 2017.

Prein, A. F., Ge, M., Valle, A. R., Wang, D., and Giangrande, S. E.: Towards a Unified Setup to Simulate Mid-Latitude and Tropical Mesoscale Convective Systems at Kilometer-Scales, Earth and Space Science, 9, e2022EA002 295, https://doi.org/https://doi.org/10.1029/2022EA002295, e2022EA002295 2022EA002295, 2022.

Pucik, T., Groenemeijer, P., Rädler, A. T., Taszarek, M., and Zanini, E.: The derecho and hailstorms of 18 August 2022, ESSL, https://www.essl.org/cms/the-derecho-and-hailstorms-of-18-august-2022/, 2022.

Púčik, T., Groenemeijer, P., Rädler, A. T., Tijssen, L., Nikulin, G., Prein, A. F., van Meijgaard, E., Fealy, R., Jacob, D., and Teichmann, C.: Future Changes in European Severe Convection Environments in a Regional Climate Model Ensemble, Journal of Climate, 30, 6771 – 6794, https://doi.org/10.1175/JCLI-D-16-0777.1, 2017.

Rehbein, A. and Ambrizzi, T.: Mesoscale convective systems over the Amazon basin in a changing climate under global warming, Climate Dynamics, 61, 1815–1827, https://doi.org/10.1007/s00382-022-06657-8, 2023.

Rigo, T., Berenguer, M., and del Carmen Llasat, M.: An improved analysis of mesoscale convective systems in the western Mediterranean using weather radar, Atmospheric Research, 227, 147–156, https://doi.org/https://doi.org/10.1016/j.atmosres.2019.05.001, 2019.

Rüdisühli, S., Sprenger, M., Leutwyler, D., Schär, C., and Wernli, H.: Attribution of precipitation to cyclones and fronts over Europe in a kilometer-scale regional climate simulation, Weather and Climate Dynamics, 1, 675–699, 2020.

Schaffer, A., Lichtenegger, T., Truhetz, H., Ossó, A., Martínez-Alvarado, O., and Maraun, D.: Drivers of Cold Frontal Hourly Extreme Precipitation: A Climatological Study Over Europe, Geophysical Research Letters, 51, e2024GL111 025, https://doi.org/https://doi.org/10.1029/2024GL111025, e2024GL111025 2024GL111025, 2024.

Schaffer, A., Lichtenegger, T., Ossó, A., and Maraun, D.: Resolution dependence and biases in cold and warm frontal heavy precipitation over Europe in CMIP6 and EURO-CORDEX models, Weather and Climate Dynamics, 6, 1815–1830, https://doi.org/10.5194/wcd-6-1815-2025, 2025.

Schumacher, R. S. and Rasmussen, K. L.: The formation, character, and changing nature of mesoscale convective systems, Nature Reviews Earth & Environment, 1, 300–314, 2020.

Stocchi, P. and Davolio, S.: Intense air-sea exchange and heavy rainfall: impact of the northern Adriatic SST, Advances in Science and Research, 13, 7–12, 2016.

Surowiecki, A. and Taszarek, M.: A 10-year radar-based climatology of mesoscale convective system archetypes and derechos in Poland, Monthly Weather Review, 148, 3471–3488, 2020.

Taszarek, M., Allen, J., Púčik, T., Groenemeijer, P., Czernecki, B., Kolendowicz, L., Lagouvardos, K., Kotroni, V., and Schulz, W.: A Climatology of Thunderstorms across Europe from a Synthesis of Multiple Data Sources, Journal of Climate, 32, 1813 – 1837, https://doi.org/10.1175/JCLI-D-18-0372.1, 2019.

Tsai, W.-M., Duan, S., O'Brien, T. A., Catto, J. L., Ullrich, P. A., Zhou, Y., Leung, L. R., Feng, Z., Boos, W. R., Suhas, D. L., Ahmed, F., and Neelin, J. D.: Co-Occurring Atmospheric Features and Their Contributions to Precipitation Extremes, Journal of Geophysical Research: Atmospheres, 130, e2024JD041 687, https://doi.org/https://doi.org/10.1029/2024JD041687, e2024JD041687 2024JD041687, 2025.